Chapter 8

Fault-Tolerant Electrical Machines and Drives

Mircea Ruba

Additional information is available at the end of the chapter

http://dx.doi.org/10.5772/67354

Abstract

The last years of research and development in the automotive industry were still focused on designing electrical propulsion units to be eco-friendly and diminish the drawbacks of classical combustion engines. Besides being energy efficient, silent, and high in power density, these must have a serious fault-tolerant ability as driver, and passengers' safety is probably the most important issue in this filed. The chapter will detail fault-tolerant machines and power electronic architectures with their control for the most common ones, such as switched reluctance machines (SRM) and the permanent-magnet synchronous machines (PMSM). Besides detection, solutions will be presented for the machine-drive unit to wisely overcome and compensate occurred faults. A novel modular structure of SRM is presented with increased fault tolerance and possibility of fast repair in case of any machine damage. The solutions will be validated via simulated and experiment-based results.

Keywords: fault tolerant, electrical machines, drives, control, fault detection, fault compensation, SRM, PMSM

1. Introduction

Electromechanical systems became in the last decade an indispensable part of nearly every electrical energy consumer. Taking advantage of the technological advance in the world of engineering, the demands in terms of performance, efficiency, reliability, and safety which were raised are continuously pushed forward [1]. Latest technological developments for such systems are based on sophisticated control strategies that have the ability to accommodate component failures automatically. By this, the system's stability is maintained in acceptable range of performances reaching what one can entitle fault-tolerant system [2].

This chapter focuses on switched reluctance and permanent-magnet synchronous machines (SRM and PMSM), dedicated for fault-tolerant applications. Modular and multiphase designs will be presented for both types of machines together with their electronic converters,

developed to serve such applications. The motivation for choosing these two electrical machines and their drives comes with the tendency of the actual market to focus research to electrify the propulsion systems in the automotive industry. Researches involved complex studies in developing solutions for fault-tolerant SRMs with their drives, solutions that are flexible and able to do online fault diagnosis and compensation [3]. Other studies were focused on electronic failure diagnosis, like the one in Ref. [4]. Winding malfunctions, such as short circuits [5] and open circuits [6], were engaged, offering solutions for intelligent control strategies. The proposed modular SRM adds to the actual status of research by a novel structural design that allows isolation and easy replacement of the faulted coils.

In the field of PMSMs, winding fault is usually the main cause of malfunctions due to short or open circuit faults. Usually, these are observed and compensated by implementing intelligent control strategies [7, 8]. Research activities were carried out also in the field of electronic faults, such as short circuit, proposing control strategies to avoid the error and try to keep the machine operational [9]. Field Programmable Gate Array (FPGA) based control methods for fault recognition and compensation based on a residual calculation were proposed in Ref. [10]. The multiphase PMSM detailed in the chapter offers a simple motor-drive fault-tolerant solution that by its architecture comes in addition to the preliminary studies.

2. Fault-tolerant switched reluctance machines and drives

By the nature of operation and by their construction, SRMs are considered up to an extent fault tolerant because these are able to operate in case of one-phase failure. However, adding to its natural fault-tolerant ability a dedicated modular stator design, one can reach a high level of safety and reliability when the application demands it. Even more, adding to such a machine a more complex electronic power converter, able to isolate and compensate the occurred fault, increases radically the fault-tolerant abilities.

The modular design of the SRM's stator consists of eight individual modules isolated between them with nonmagnetic displacers as shown in **Figure 1**. One machine phase is compounded of the coils wound on diametrically opposed modules. These are fixed to the end caps of the machine using nonmagnetic rods that pass through them. Using the nonmagnetic displacers between adjacent modules, the magnetic flux's path is forced only via the energized module and the corresponding rotor poles as seen in **Figure 1**. The machine's rotor is a classical design having 14 poles.

The concept regards that the coils of each phase are fed independently. In this case, with independent supply and because one stator slot is not shared by coils from different phases, in case of short circuits, overheating, etc. of one coil, the remaining ones are not influenced nor altered.

This way, if a coil of one phase is faulted, the machine will continue operating with the remaining diametrically opposed coil. This event can occur from one to all phases of the machine, and it can still operate in satisfactory conditions. One solution to compensate the faulted coils, is to increase the current of the remaining healthy ones. This is allowed by

http://dx.doi.org/10.5772/67354

their design, even if it will mean saturation of the core and increase of the machine's temperature. It is easy to understand that the developed torque and speed in case of fault will be lower than in normal condition but, still, will reach satisfactory values till safe stop of the machine is possible.

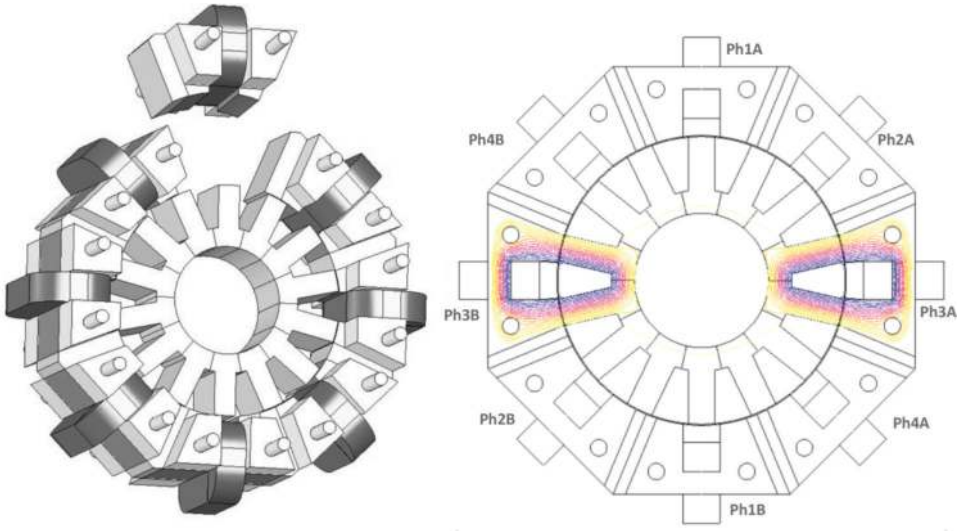

Figure 1. The 3D model of the modular SRM and its flux paths on one phase and the coil distribution.

This design allows besides isolation of the coils and of the magnetic cores simple and fast replacement of the damaged modules with new ones. Extracting the fixing rods permits removal of the nonfunctional modules without the need of uncoupling the shaft from the application and without moving the machine out of its housing. The prototype built to prove the concept was rated at 300 Vdc, 6 A, 600 rpm, and 5 Nm, as specifications for the design process.

2.1. The design of the modular SRM

Due to the fact that the machine has nonclassical features, its design process is based on an analytical model combined with particular calculations required by the modular structure. The number of rotor poles (Q_R) is a function of the number of stator modules (N_{mS}) and the number of phase to coil division (n_{div}):

$$Q_R = n_{div} \cdot N_{mS} - n_{div} \tag{1}$$

The design process followed complex algorithms [11–13] to shape the geometry of the core assemblies but at the same time, to size and determine the machine's characteristics such as torque, losses, flux densities, etc.

The shaping process starts by imposing several parameters that will characterize the performances of the future machine. These regard the supply voltage (U_N), the rated current (I), the number of phases (m), the machine's rated power (P_{2N}), the mechanical air gap (g), the air-gap flux density in aligned position (B_{gmax}), the rated speed (n_N), and the rated torque (T_N).

For any SRM, classical or modular one, the most important parameter that has important influence on its performances is the mean diameter, as value measured in the middle point of the air gap [14]:

$$D_g = \sqrt[3]{\frac{P_{2N} \cdot Q_s \cdot k_\sigma}{Q_R \cdot \pi^2 \cdot k_L \cdot \frac{n_N}{60} \cdot B_{g\max} \cdot \left(1 - \frac{1}{K_{cr}}\right) \cdot A_S}} \tag{2}$$

where (Q_S) and (Q_R) are the numbers of stator and rotor poles. Coefficients (k_σ) and (k_L) regard the leakage flux factors, as values between 0.75 and 0.95, the aspect factor, respectively, are calculated like

$$k_L = \frac{\pi}{2} \cdot \frac{1}{\sqrt[3]{Q_R}} \tag{3}$$

The electrical loading A_S will be chosen in an interval between 5^4 and 15^4 A/m, while Carter's factor K_{CR} considers the shape of the salient poles and the flux path's distortion due to this shape [15]. It is chosen in a range between 1.4 and 2.

Computing the ratio of the mean diameter (D_g) with respect to the aspect of coefficient yells for a preliminary value of the machine's active stack length (l_a) that can be later adjusted as function of the resulted developed torque. Usually, this value can be restricted by the housing of the machine.

Because the stator is compounded of eight independent modules, it is enough to size only one of them. The complete circle described by the inner stator diameter is split into (N_{mS}) arcs, equal with the number of the stator modules. The length of one arch described by one module is

$$L_m = \frac{2 \cdot \pi \cdot \left(\frac{D_g}{2} + \frac{g}{2}\right)}{N_{mS}} \tag{4}$$

The SRM by its nature due to its saliency and due to its switched current operation has the well-known torque ripples, influenced also by the saturation of the pole tips. When discussing about analytical calculation of the mean torque, it is quite difficult to take into account all the factors. Hence, as the most influential parameter on the torque development is the core saturation, instead of the geometrically defined air gap (g), an equivalent value will be used in the following calculations, the latter considering the saturation of the poles in aligned position by (k_{sat}) coefficient:

$$g_x = k_{sat} \cdot g \tag{5}$$

To ensure correct isolation between the modules, it was considered necessary that the spacers between them (l_D) should be at least 10 but not larger than 20 times the air gap.

http://dx.doi.org/10.5772/67354

The arch defined by one stator module (see **Figure 2**) computed with Eq. (4) includes also the arch defined by the spacer. Hence, the pole pitch described just by the module itself without the spacer is half of the difference between (L_m) and (l_D):

$$\tau_S = \frac{L_m - l_D}{2} \tag{6}$$

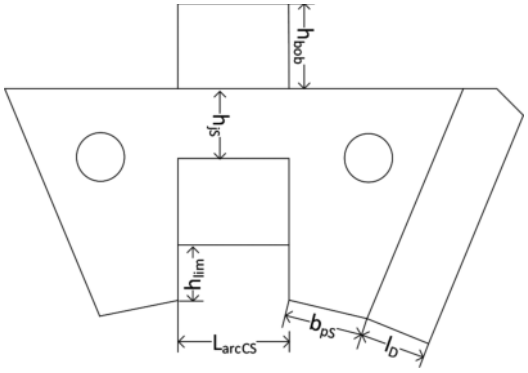

Figure 2. Sizing the stator module.

Sizing the width of the stator poles is based on ranging their values between 0.5 and 0.8 of the module total pitch. The value has to be considered in order to leave space to fit the winding and to ensure correct overlapping with the rotor poles. Round values are indicated to be used, as it simplifies the building process. Hence, the stator pole width was considered to be

$$b_{pS} = round(0.58 \cdot \tau_S) \tag{7}$$

Finalizing the computation of the stator pole width requires to recompute the value of the spacers between the modules, in order to close the circle described by the inner stator radius. By now, only a preliminary value of the spacer was considered. Before proceeding to this calculation, firstly the rotor pole pitch has to be computed:

$$L_{arcPR} = \frac{\pi \cdot \left(\frac{D_g}{2} - \frac{g}{2}\right) \cdot \frac{360}{Q_R}}{180} - 2 \cdot \frac{b_{pR}}{2} \tag{8}$$

where b_{pR} is the rotor pole width, considered equal with the stator pole width (b_{pS}). To calculate the real dimensions of the spacer, the stator slot opening width (L_{arcCS}) needs to be computed:

$$L_{arcCS} = round\left(\frac{\pi\left(\frac{D_g}{2} + \frac{g}{2}\right) \cdot u_C}{180}\right) \tag{9}$$

where (u_C) is the angle described by the rotor pole pitch arc, calculated as

$$u = \frac{\pi \cdot \left(\frac{D_s}{2} - \frac{g}{2}\right) - \frac{360}{Q_R} - b_{pS}}{\pi \cdot \left(\frac{D_s}{2} - \frac{g}{2}\right)} \tag{10}$$

To finalize the sizing of the module spacers, it is considered that the stator and rotor slots are equal and the distance between them is just the air gap. Hence, the spacer can be sized as

$$l_D = L_m - 2 \cdot b_{pS} - L_{arcCS} \tag{11}$$

By now, only the module's yoke height remains to be sized. To make sure that proper saturation is reached advantaging fast demagnetization when the phase is switched in *off* state, the yoke was considered to be 0.85 of the pole's width:

$$h_{jS} = round\left(0.85 \cdot b_{pS}\right) \tag{12}$$

Because no information is yet available about the size of the coils that need to be fitted inside the stator slot, only a preliminary value can be considered to the height of the stator poles, simply obtained as

$$h_{pS} = round(1.01 \cdot L_m) \tag{13}$$

This value will be recomputed after sizing the coils. However, the active stator pole surface will be

$$A_{pS} = b_{pS} \cdot l_a \tag{14}$$

Before sizing the coils, which will require information about the length of the flux paths, the rotor must be sized. As already stated, the rotor pole pitch is equal with the one of the stator. As the width of the rotor poles are also at the same size as the one of the stator poles, one can compute the rotor slot opening like

$$b_{cR} = round\left(L_{arcR} - b_{pR}\right) \tag{15}$$

As seen in **Figure 1**, the magnetic flux closes only via the energized module and the corresponding rotor poles; hence, the yoke of the rotor (h_{jR}) can be considered equal with the one of the stator (h_{jS}). Imposing the diameter of the machine's shaft (d_{ax}), it is possible to compute rotor pole height (see **Figure 3**):

$$h_{pR} = round\left(\frac{D_g}{2} - \frac{g_x}{4} - h_{jR} - \frac{d_{ax}}{2}\right) \tag{16}$$

As mentioned earlier, after sizing the rotor, it is possible to compute the dimensions of the coils in relation with the magnetic field (H) and the machine's geometrical dimensions.

To be able to compute the required magnetomotive force, the length of the flux paths through the stator (l_s), air gap (l_g), and rotor (l_r) must be calculated:

http://dx.doi.org/10.5772/67354

$$\begin{aligned} l_s &= 2 \cdot h_{pS} + L_{arcCS} \\ l_g &= 2 \cdot g \\ l_r &= 2 \cdot h_{pR} + L_{arcCR} \end{aligned} \tag{17}$$

Based on Ampere's law, it is easy to compute the magnetomotive force, and from there the number of turns per coil N_f is

$$\begin{aligned} \Theta &= H_{Fe} \cdot (l_s + l_r) + H_g \cdot l_g \\ N_f &= round(\Theta / I) \end{aligned} \tag{18}$$

Function of the desired current and the number of turns, one can easily determine the size of the coil (h_{bob}) that will allow the final computation of the height of the stator module:

$$h_m = h_{\lim} + h_{bob} + h_{jS} \tag{19}$$

Having all the abovementioned data, sizing process of the machine is finished. To validate the breviary, the designer has to compute the developed mean torque using

$$T_v = k_{unal} \cdot N_{op} \left(N_f \cdot I\right)^2 \cdot \frac{D_g}{2} \cdot \mu_0 \cdot \frac{l_a}{4 \cdot g_x} \tag{20}$$

where (N_{op}) is the number of modules of one phase and (k_{unal}) is a constant that considers the contribution of the magnetic flux in unaligned position.

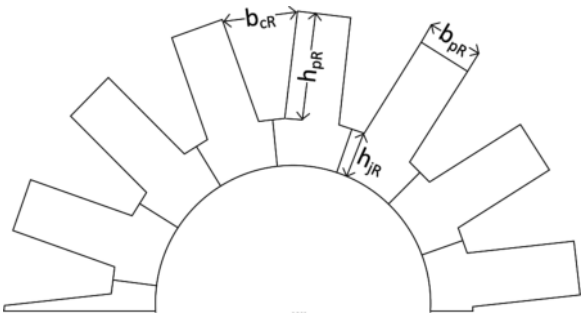

Figure 3. Sizing the rotor of the machine.

2.2. The operation of the fault-tolerant SRM

Validation of the modular SRM's design was accomplished via both finite element simulations and experimental testing in the laboratory. In both cases, the electronic converter had half-H bridges for each coil like in **Figure 4**. Hence, the two coils of one phase had each an independent half-H bridge (e.g., phase Ph1 is compounded of two independently but synchronously supplied coils, Ph1A and Ph1B). The concept was to permit the converter and the controller to separate and compensate the faulted coils. During normal operation, the coils of one phase were supplied with the same current using hysteresis current controller.

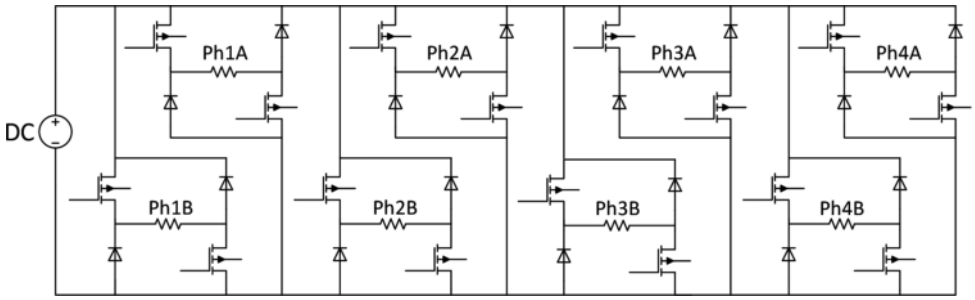

Figure 4. The electronic converter's topology.

It is clear that in case of any fault, the controller stops feeding with current the damaged coil and supplies only the healthy remaining one. This structure is indeed a more complex one than in the case of classical converters, but it is motivated by the highly increased fault-tolerant application of the machine.

Using Flux2D software, several tests were performed in both healthy and faulty conditions with 1–4 open circuit coils. In **Figure 5(a)**, **(b)**, and **(c)**, the healthy condition is depicted. The currents are plotted separately for all the eight coils of the machine (coils Ph1A, Ph2A, Ph3A, and Ph4A in plot b) and (coils Ph1B, Ph2B, Ph3B, and Ph4B in plot c). The developed RMS torque is 5.7 Nm at the rated current of 6 A. In case of one faulted coil (open circuit of Ph1A of phase 1), as it can be seen in **Figure 5d**, correspondence to the missing coil's (**Figure 5e**) current of the torque falls, being generated only by Ph1B of phase 1. Due to separate supply of the two coils of the phases (see **Figure 4**), Ph1B remains operational, as it is depicted in **Figure 5f**. The machine continues to operate even if the ripples are increased. It has to be mentioned also that all the tests were carried out only with classical hysteresis control strategy just to prove the machine's operational skills.

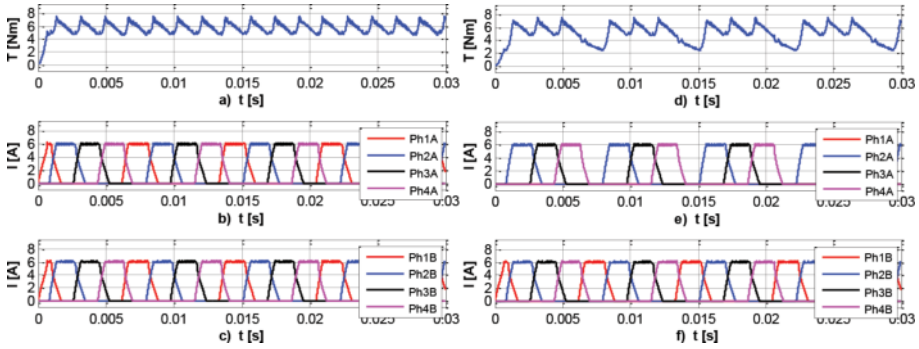

Figure 5. Finite element simulation results in healthy (a–c) and one-coil open fault (d–f).

In case of more sever faults, as it can be seen in **Figure 6** for two to four opened coils, the RMS torque decreases and yells for more ripples, still the machine being able to perform continuous operation.

http://dx.doi.org/10.5772/67354

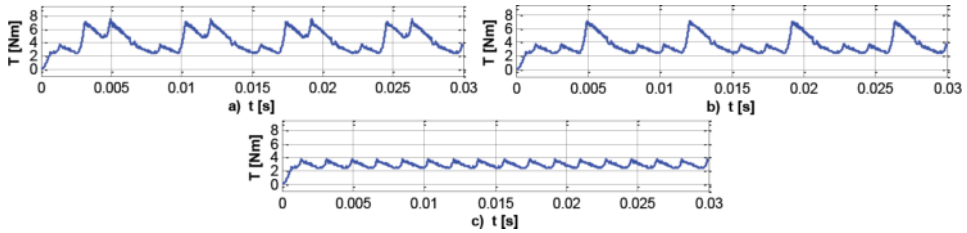

Figure 6. Simulated results in faulted conditions: two coils (a), three coils (b), and four coils (c).

The experimental validation of the concept and of the machine itself was accomplished by building the modular SRM with regard to the design specifications and setting up a test bench like the one in **Figure 7**. The modules were cut out of lamination and fixed into an aluminum housing. The test bench was compounded of the SRM, an induction machine as a load, a torque meter, the complex converter, and a dSPACE 1104 card for its control. An encoder was mounted on the shaft of the machine to provide feedback of the speed and the rotor position. To prove the operational skills of the machine, the same tests were carried out on the test bench like those performed in simulations.

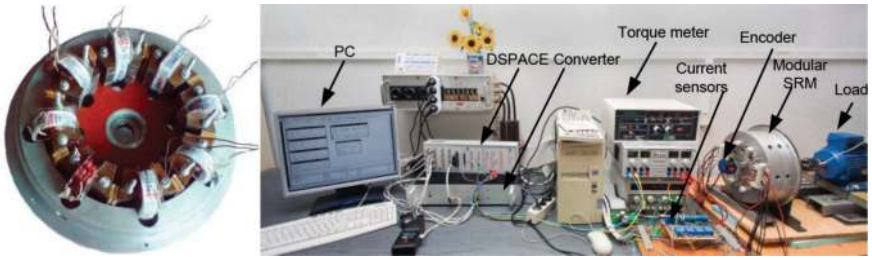

Figure 7. The modular stator of the SRM (left) and the experimental test bench (right) [8].

The experimental results depicted in **Figure 8(a)** to **(c)** in healthy condition and **Figure 8(d)** to **(f)** in open fault condition prove that the machine reaches the same performances as in simulations. As the measured results are quite close to the ones obtained in simulations, the same explanations that were detailed with regard to **Figure 5** are valid for the measured results.

In **Figure 9**, the results for faulted condition in experimental testing are depicted. The same remarks described for the simulated results of each fault scenario are valid also for the measured ones. By this, it was proved that the design breviary and the experimental model of the SRM are in accordance and the machine reaches the desired performances. In case of faults, if the currents on the remaining coils are not increased, the torque ripples are intensified. However, the machine can continue its operation even if four of the eight coils are not operational. The slight differences between the simulated results in **Figure 5** and those obtained in real measurements in **Figure 8** are due to low sampling speed and quite low precision in rotor position measurement, as an encoder was used instead of a resolver.

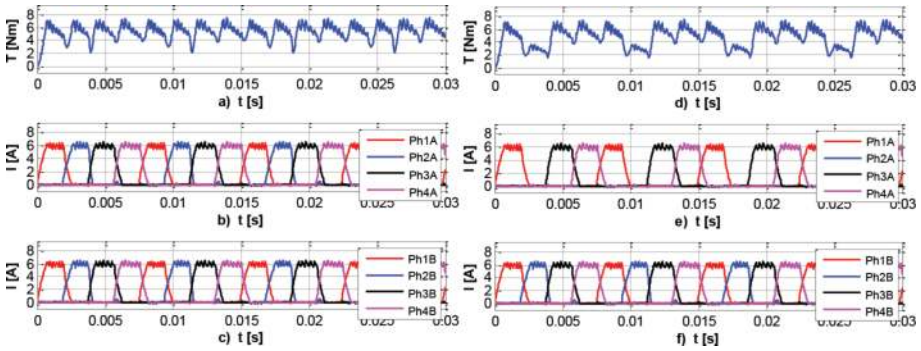

Figure 8. Experimental results in healthy (a–c) and one-coil open fault (d–f).

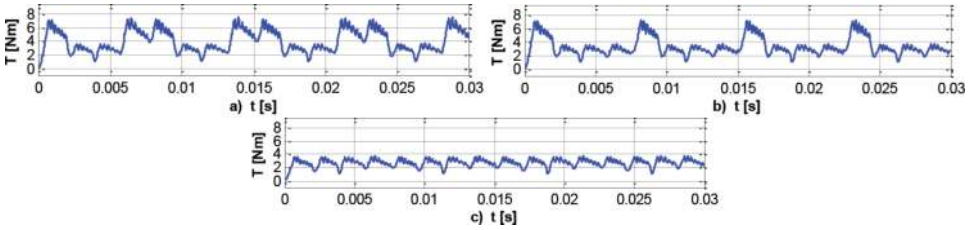

Figure 9. Experimental results in faulted conditions: two coils (a), three coils (b), and four coils (c).

Comparing the results obtained from simulations and those obtained in experimental testing, one can conclude that even in faulty condition, the machine reaches quite good performances. Comparing the results gathered in **Table 1**, it can be stated that there are quite good agreements between them. The biggest difference was reached in four opened coil conditions, about 0.65 Nm. However, in any fault condition, the SRM is able to develop more than 60% of the rated torque, this correspondence to the worst case scenario (four opened coils).

	RMS torques (N·m)	
Condition	**Simulated**	**Measured**
Healthy machine	5.5	5.3
One faulted coil	4.9	4.68
Two faulted coils	4.34	4.05
Three faulted coils	3.8	3.32
Four faulted coils	3.3	2.65

Table 1. The RMS torque obtained in simulated and experimental analysis.

http://dx.doi.org/10.5772/67354

Proving the concept and the operational skills, it is worth mentioning that, due to simple hysteresis control strategy, in case of faults, the torque ripples are quite high. However, engaging torque-smoothing strategies, such as direct instantaneous torque control or current profiling, it is possible to reach satisfactory torque characteristic, quite close to a linear one [9, 10], even in case of fault operation.

3. Fault-tolerant permanent-magnet synchronous machines and drives

The PMSMs due to their high power density, maturity, and reliability became in the last decade more and more used in all the fields of electromechanical systems. Many applications such as aircrafts, military, medicine, electric propulsion, etc. embed such machines, demanding in the same time high fault-tolerant capabilities. Hence, fault-tolerant PSMSs became a hot topic. Investigating ideas like six-phase inverters with common mode voltage elimination [16], or using series-connected six-phase inverter with a three-phase motor to use the same inverter for two machines [17] or adding a supplementary leg to the three-phase inverter, used only in faulty condition [18, 19] became widely used solutions for fault PMSM-tolerant applications. However smart-design considerations [20, 21] and dedicated control strategies [22, 23] were applied to increase the fault-tolerant potential of the machine.

In order to achieve a more increased level of fault tolerance, a nine-phase PMSM is proposed supplied from a special electronic converter able to overcome and compensate the occurred fault, like the one in **Figure 10**. The design of the machine, the power converter, and their operation will be described in the following, highlighting the benefits of using such a complex but fault-free system.

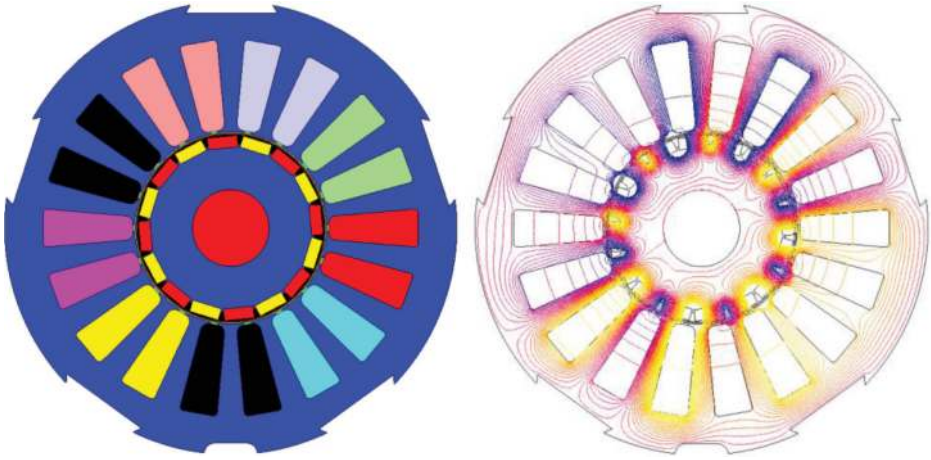

Figure 10. The structure of the nine-phase PSMSM (left) and its flux paths (right).

3.1. The design of the nine-phase PMSM

Taking into account published solutions to reduce significantly the torque ripples using fractional-slot winding configuration [24, 25], a PMSM with 8 pole pairs and 18 slots was designed. The machine has nine phases, and in the addition to classical designs, each phase is formed by one coil that surrounds only one tooth. Hence, the phases are magnetically separated, increasing its reliability by diminishing the influence of one faulted phase over the remaining healthy one. The ratings for this machine are 48 Vdc, 500 rpm, 1.8 Nm, and 66.6 Hz of fundamental current frequency.

The sizing process is based on a generalized algorithm that one can use for any type of PMSM indifferent of the number of phases, slots, or pole pairs. Neglecting the leakage reactance, the output power can be a computed function of the estimated efficiency (η), the number of phases (n_{ph}), the peak value of the mmf (E_{max}), and the peak value of the phase current (I_{max}):

$$\begin{aligned} P_{out} &= \eta \cdot n_{ph} \cdot E_{\max} \cdot I_{\max} \\ Q_R &= n_{div} \cdot N_{mS} - n_{div} \end{aligned} \tag{21}$$

In Eq. (22), the peak value of the mmf can be a computed function of its coefficient (k_E), the number of turns per phase (N_t), the air-gap flux density (B_{gap}), the active stack length (L_m), the supply current frequency (f_s), and the number of pole pairs (p):

$$E_{\max} = k_E \cdot N_t \cdot B_{gap} \cdot L_m \cdot f_s / p \tag{22}$$

Defining the geometric coefficient, $k_L = L_m/D_{gap}$, the current coefficient $k_i = I_{max}/I_{rms}$, and defining the phase load in ampere-turns:

$$A_t = 2/\pi \cdot N_t \cdot I_{rms}/D_{gap} \tag{23}$$

One can compute the air-gap mean diameter, just like for the SRM in Eq. (2), using

$$D_{gap} = \sqrt[3]{\frac{2 \cdot p \cdot P_{out}}{\pi \cdot n_{ph} \cdot A_t \cdot k_E \cdot k_i \cdot k_L \cdot \eta \cdot B_{gap} \cdot f_s}} \tag{24}$$

Based on the value computed with Eq. (23), it is possible to size all the rest of geometrical dimensions of the machine, based on classical models. The resulting air-gap flux density can be determined with

$$B_{gap} = \frac{h_m \cdot B_{rm}}{\frac{D_{gap}}{2} \cdot \left(\ln\left(\frac{R_{si} - gap}{R_{cr}} \right) + \ln\left(\frac{R_{si}}{R_{si} \cdot gap} \right) \right)} \tag{25}$$

where (h_m) is the length of the permanent magnet, (B_{rm}) is the permanent magnet's remanent flux density, (R_{si}) is the stator inner diameter, (R_{cr}) is the rotor core diameter, and (gap) is the air-gap length. The rest of the electromagnetic parameters can be computed based on the air-gap flux density. The phase emf, proportional with the frequency and the number of turns,

the flux linkage, and the demagnetization coefficient (k_d) given by the permanent magnet's specifications (around 0.8–0.9) can be determined:

$$E_{ph} = \sqrt{2} \cdot \pi \cdot f_s \cdot N_t \cdot k_{ws} \cdot \Psi_m \cdot k_d \tag{26}$$

where (k_{ws}) is the winding coefficient, specific for the used winding type.

The PMSM's speed is given proportional with the emf and inverse proportional with its coefficient:

$$\begin{aligned} \Omega &= E_{ph}/k_E \\ T_m &= P_{out}/\Omega \end{aligned} \tag{27}$$

The developed mean torque is a computed function of the output power and the machine speed. All that remain now, having the machine designed, are to validate its operation both in simulations and in laboratory measurements.

3.2. The operation of the nine-phase PMSM

Before proceeding to validation of the machine, it is important to describe the dedicated electronic power converter attached to the machine and the concept of its control, in order for the reader to be able to understand the choice of the system's assemblies.

One solution for a converter to be fault tolerant is to create H bridges around each phase and control them independently. However, such a structure is very expensive, and at the same time, it is quite difficult to create its proper control. A cost-effective solution is to build a converter like the one depicted in **Figure 11**. The concept of the inverter is to divide the nine phases of the machine in three groups of three phases [24, 25]. Each group of three phases forms a star connection obtaining a neutral point that is connected to an additional inverter leg. This is operated only if fault occurs on one of the three phases of one star. By this, the machine can be operated even if three phases are faulted, with only one of the three sets of phases. Moreover, even if one of the last three remaining phases is faulted, the machine can continue its operation with only two of the nine phases.

In case the fault occurs on one phase of a group of 3, this is automatically isolated by keeping the power switches around it open. However, due to the imbalance, the zero sequence current is not null anymore. To keep the balance, this current, (I_0), has to reach the supply. This is where the additional leg is operated, ensuring that the zero sequence current reaches the supply and by this, practically, the remaining healthy phases keep their balance driving normal currents to the machine.

In order to have a better understanding of the phenomenon, the discussion that follows will be held on a system of three-phase currents. However, as practically the three-phase machine has 3×3 phases, the concept is extendable applying the same procedures.

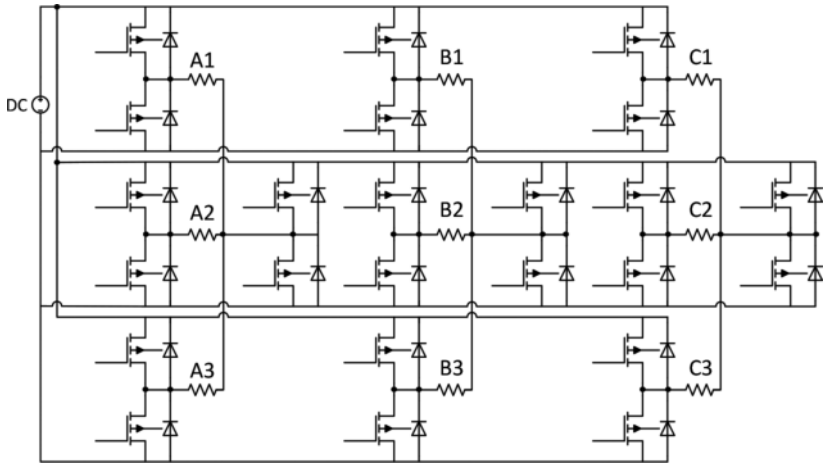

Figure 11. The nine-phase fault-tolerant inverter structure.

In a three-phase system, the currents in a rotating reference frame are governed by

$$\begin{aligned} I_a &= I_d \cdot \sin(\omega t) + I_q \cdot \cos(\omega t) + I_0 \\ I_b &= I_d \cdot \sin\left(\omega t - 2\frac{\pi}{3}\right) + I_q \cdot \cos\left(\omega t - 2\frac{\pi}{3}\right) + I_0 \\ I_c &= I_d \cdot \sin\left(\omega t + 2\frac{\pi}{3}\right) + I_q \cdot \cos\left(\omega t + 2\frac{\pi}{3}\right) + I_0 \end{aligned} \tag{28}$$

Writing those in fixed reference frame will give

$$\begin{aligned} I_a &= \frac{3}{2} I_\alpha + \frac{\sqrt{3}}{2} I_\beta \\ I_b &= \sqrt{3} I_\beta \\ I_c &= 0 \end{aligned} \tag{29}$$

The electromagnetic torque in general relation is expressed as

$$T_m = \frac{3}{2} \cdot p \cdot \left(I_q \cdot \Psi_m + \left(L_d - L_q\right) \cdot I_d \cdot I_q\right) \tag{30}$$

In relation to Eq. (30), it can be seen that to maintain a constant torque, the dq components of the currents must remain the same. The link between fixed and rotating referenced frame currents is given by

$$\begin{aligned} I_\alpha &= I_d \cdot \cos(\omega t) - I_q \cdot \sin(\omega t) \\ I_\beta &= I_d \cdot \sin(\omega t) + I_q \cdot \cos(\omega t) \end{aligned} \tag{31}$$

Hence, substituting Eq. (31) into Eq. (29) gives the three-phase current law needed to keep the developed electromagnetic torque constant:

http://dx.doi.org/10.5772/67354

$$\begin{aligned} I_a &= \sqrt{3}I_d \cdot \sin\left(\omega t + \frac{2\pi}{3}\right) + \sqrt{3}I_q \cdot \cos\left(\omega t + \frac{2\pi}{3}\right) \\ I_b &= \sqrt{3}I_d \cdot \sin(\omega t) + \sqrt{3}I_q \cdot \cos(\omega t) \\ I_c &= 0 \end{aligned} \tag{32}$$

Eq. (32) proves that the machine can keep the developed torque constant only if the currents are increased with $\sqrt{3}$. However, if the currents are not increased, in case of fault, the machine will develop only 2/3 of the rated torque. This concept demonstrates that, in case of faults, the machine can be supplied to develop the same torque by controlling the magnitude of the *dq* currents. It has to be mentioned that for such applications, the winding must be sized properly, to be able to handle increased currents without the risk of burnout.

Validation both in simulations and in laboratory experiments will be focused on injecting currents in the neutral point using the additional inverter leg, to compensate the fault occurred in each star connection of the machine.

Flux2D software, a software based on finite element analysis, was used to validate the machine via simulations.

In **Figure 12** the normal and one-phase fault conditions are depicted for the nine-phase PMSM. As it can be seen for the normal condition, all the nine currents are present developing torque, reaching 1.8 Nm, the rated value. In case of fault, this was set to occur at 0.01 s; it can be seen that the lack of one phase creates torque ripples and its RMS value diminishes to 1.6 Nm. In order to prove the concept, no currents will be increased, highlighting that the value of the torque is diminished with 2/3 for each phase.

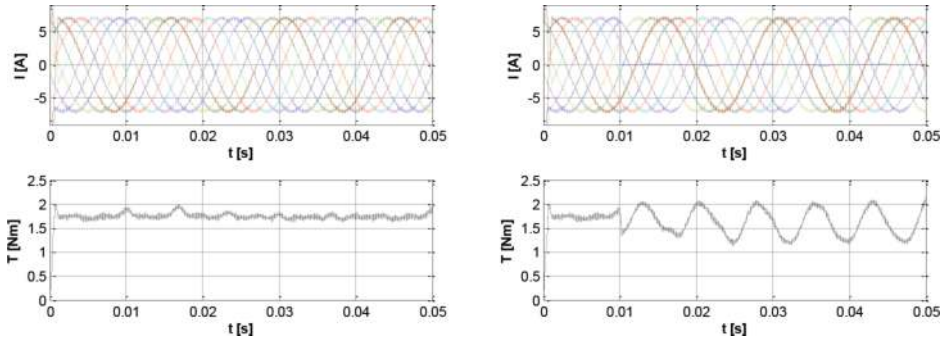

Figure 12. Simulated result in healthy (left) and one-phase fault (right).

Figure 13 depicts several fault condition tests that were performed. When two phases from two star connections are lacking (**Figure 13**, top-left), the torque ripples increase even more, and the RMS value reaches 1.5 Nm. If a third phase (**Figure 13**, top-right), from the third star connection, is faulted, the ripples increase again, and the RMS value of the torque decreases to 1.35 Nm. The worst case scenario is depicted in **Figure 13** (bottom). Here, two phases from one star and one from each of the other stars are faulted. Hence, only five phases remain

operational in the machine. High torque ripples are reached in this case, and the torque developed barely passes 1 Nm as mean value.

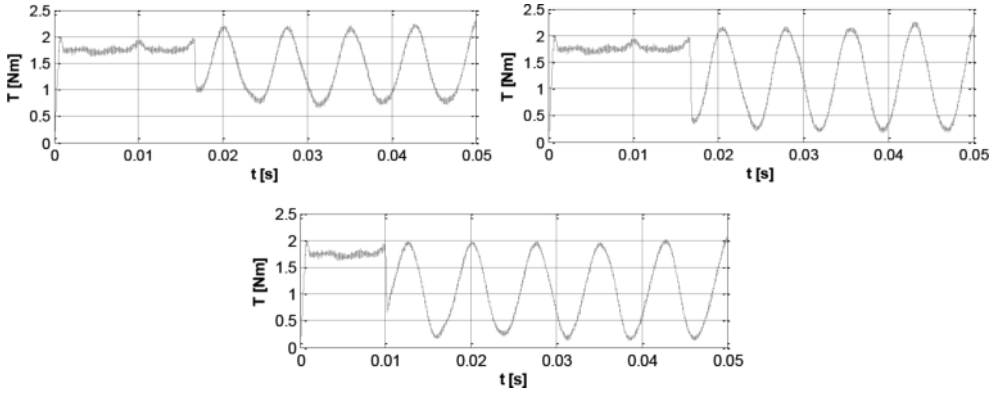

Figure 13. Simulated results in faulted conditions: two phases (top-left), three phases (top-right), and four phases (bottom).

The experimental validation of the nine-phase PMSM was done with the test bench depicted in **Figure 14**. Its main assemblies are the PMSM, a torque meter, an induction machine as load, the complex electronic converter, nine current sensors, a power supply, and a dSPACE 1103 card for the control [16].

Figure 14. The nine-phase PMSM test bench.

In order to highlight the benefit of using the additional leg of each star connection, a debate will be focused on only one of the three star connections, the phenomenon being the same for the entire machine. The three-phase currents and the developed torque in healthy condition are depicted in **Figure 15** (top). The amplitude of the currents and torque reaches rated values; these are being measured at the rated speed. The deformation of the currents is given by low

http://dx.doi.org/10.5772/67354

switching frequency. The developed torque is about 1.72 Nm as RMS value, quite close to the one obtained in simulations. In case of a phase fault of one star (obtained by forcing open circuit), without engaging the fourth leg, the currents become shifted with 180°, like in **Figure 15** (middle). However, engaging the fourth leg, this will complete the switching table of a three-phase system, keeping the currents shifted with the proper angle.

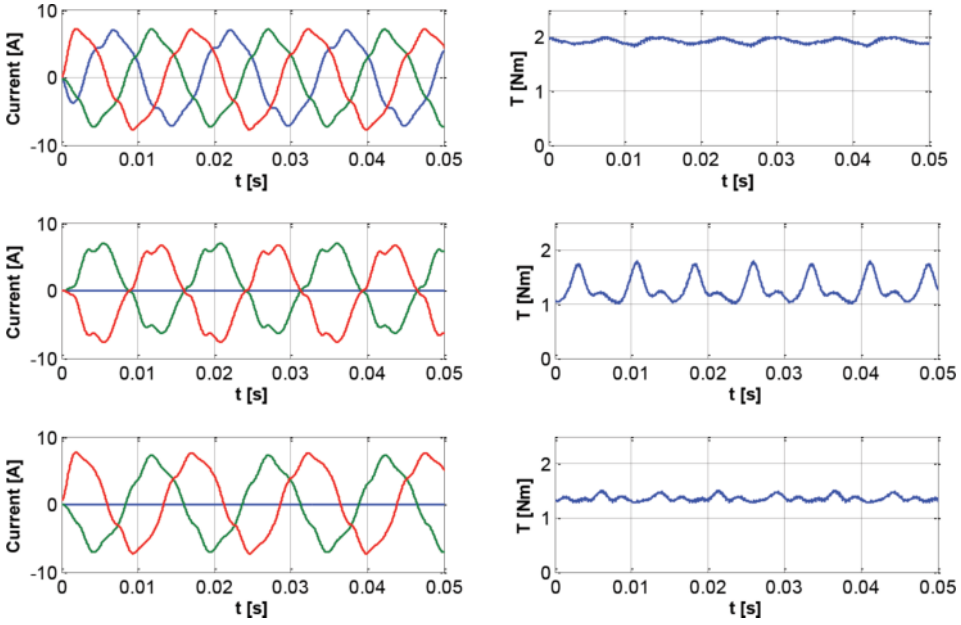

Figure 15. The currents (left) and the instantaneous torque (right) for healthy machine (top) and in one-phase fault without (middle) and with (bottom) the contribution of the fourth leg.

The torque is diminished in this case, but the ripples are much lower than in the case when the fourth leg was not engaged. The RMS torque obtained was 1.62 Nm, quite close to the one resulted simulations wise.

This analysis proves the benefits of using such a configuration of an additional fourth leg correspondence for each group of three phases in star connection. This operational concept is extendable for any number of phases. As the machine in study has nine phases, the same fault conditions that were tested in simulations will be applied in the experimental validation too.

In **Figure 16**, nine-phase currents are plotted for healthy machine operation. The reason of the distortion was already explained in the above paragraphs. To compare the results with those obtained in simulation, firstly two phases are opened from two different star connections. It can be seen in **Figure 16** (top-right) that for this condition the torque ripples are higher than in the case of only one phase fault. The RMS torque developed was about 1.42 Nm. Another fault condition was to open three phases, each from a different star connection. The result plotted in **Figure 16** (bottom-left) shows not only the high torque ripples but also some instability of the

characteristic. In this case about 1.28 Nm RMS torque was developed. The worst case scenario is having two opened phases from the first star connection and other two phases from each of the remaining stars. The torque depicted in **Figure 16** (bottom-right) presents the highest torque ripples and an RMS torque of 1.18 Nm. Comparing the results from simulations and from experimental measurements in the same operation conditions, there are quite consistent differences between them. The reasons are due to the fact that the analysis conditions were quite different. The switching frequency during experiments was limited to the computation power of dSPACE. By this, the shape of the currents included a certain content of harmonics that has direct impact on the shape of the torque. The rotating assemblies of the test bench had consistent inertia adding together one of the loads of the mechanical coupling and of the PMSM's itself. Overall, the analysis highlighted the benefits of using a fractional-slot design for the machine to diminish the torque ripples supplied by a special electronic converter able to isolate and compensate the faults. The level of fault tolerance was proven by the fact that the machine is able to operate with only five of its nine phases, continuing to develop quite a reasonable quantity of torque.

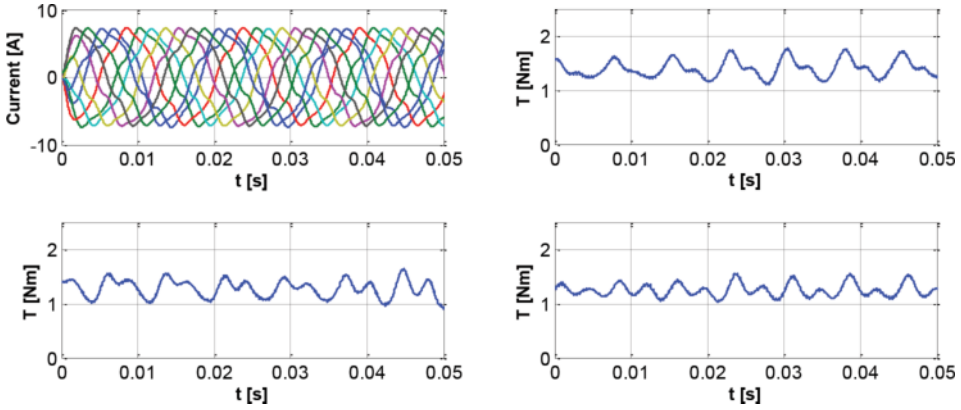

Figure 16. The nine-phase currents (top-left) and the instantaneous torque for fault on two star connections (top-right), fault on three star connections (bottom-left), and fault on two phases of a star and fault of one phase of each of the other two stars (bottom-right).

4. Conclusions

In the present chapter, fault-tolerant electrical machines and drives are presented for particular applications in the light electric vehicle industry. The goal was to analyze the most used machine nowadays in this area such as the switched reluctance and the permanent-magnet synchronous machines. The latter one was designed in a multiphase structure, having nine-phases, each three of them connected in a star connection. Operating this machine with a dedicated special architecture electronic converter, one can reach continuous operation despite open-phase conditions. Numerical simulations and experimental tests prove the operational skills of the machine.

The fault-tolerant SRM was designed in a novel concept, to have a modular stator, each module caring independent coils. Each diametrically opposed two coils form one stator phase, but each coil is supplied independently from a half-H bridge. For this machine also numerical and experimental studies proved the integrity and the usefulness of the machine.

The presented structures are part of a step forward in the field of high reliability electrical machines. These, controlled with the proposed electronic converters and adding intelligent control strategies, are able to reach high fault-tolerant capabilities. On the other hand, considering the price of implementing such structures, it is clear that these are higher than the classical ones. However, fault-tolerant systems are by default high-cost designs, and these costs are increasing with their complexity and reliability.

Author details

Mircea Ruba

Address all correspondence to: mircea.ruba@emd.utcluj.ro

Technical University of Cluj Napoca, Romania

References

[1] B. Tabbache, A. Kheloui, M. Benbouzid, A. Mamoune, D. Diallo. "Research on Fault Analysis and Fault-Tolerant Control of EV/HEV Powertrain," in IEEE ICGE 2014, Mar 2014, Sfax, Tunisia. pp. 284–289.

[2] Y. Zhang, J. Jiang. "Bibliographical review on reconfigurable fault-tolerant control systems," ELSEVIER, Annual Reviews in Control, vol. 32, 2008, pp. 229–252. DOI: 10.1016/j.arcontrol.2008.03.008

[3] Y. Hu, C. Gan, et al. "Flexible fault-tolerant topology for switched reluctance motor drives," IEE Transactions on Power Electronics, vol. 31, no. 6, 2016, pp. 4654–4668.

[4] N. S. Gameiro, A. J. Marques Cardoso. "A new method for power converter fault diagnosis in SRM drives," IEEE Transactions on Industrial Applications, vol. 48, no. 2, 2012, pp. 653–662.

[5] B. Lequesne, S. Gopalakrishnan, A. M. Omekanda. "Winding short circuits in the switched reluctance drive," IEEE Transactions on Industrial Applications, vol. 41, no. 5, 2005, pp. 1178–1184.

[6] W. Ding, Y. Liu, Y. Hu. "Performance evaluation of a fault-tolerant decoupled dual-channel switched reluctance motor drive under open-circuits," IET Electric Power Applications, vol. 8, no. 4, 2014, pp. 117–130.

[7] C. J. Gajanayake, B. Bhangu, et al. "Fault tolerant control method to improve the torque and speed response in PMSM drive with winding faults," 2011 IEEE Ninth International Conference on Power Electronics and Drive Systems (PEDS), 5–8 Dec. 2011. DOI: 10.1109/PEDS.2011.6147371

[8] O. Wallmark, L. Harnefors, O. Carlson. "Control algorithms for a fault-tolerant PMSM drive," IEEE Transactions on Industrial Electronics, vol. 54, no. 4, 2007, pp. 1973–1980. DOI: 10.1109/TIE.2007.895076

[9] N. K. Nguyen, F. Meinguet, E. Semail, X. Kestelyn. "Fault-tolerant operation of an open-end winding five-phase PMSM drive with short-circuit inverter fault," IEEE Transactions on Industrial Electronics, vol. 63, no. 1, 2016, pp. 595–605. DOI: 10.1109/TIE.2014.2386299

[10] H. Berriri, M. Naouar, I. Slama-Belkhodja. "Easy and Fast Sensor Fault Detection and Isolation Algorithm for Electrical Drives," IEEE Transactions on Power Electronics, vol. 27, no. 2, Feb. 2012, pp. 490–499. ISSN: 1941-0107

[11] I. A. Viorel, S. Larisa, I. F. Soran, "Analytical flux linkage model of switched reluctance motor," Romanian Journal of Technical Sciences – Electrotechnical And Energy Series, vol. 54, no. 2, 2009, pp. 139–146.

[12] G. Henneberger, I. A. Viorel. "Variable Reluctance Electrical Machines." Shaker Verlag, Aachen (Germany), 2001.

[13] A. Radun. "Design considerations for the switched reluctance motor," Proceedings of IEEE Transactions on Industrial Applications, vol. 31, no. 5, 1995, pp. 1079–1087.

[14] R. Krishnan. "Switched Reluctance Motor Drives – Modeling, Simulation, Analysis, Design, and Applications." Industrial Electronics Series, CRC Press, Alabama, USA, 2001. ISBN 0-8493-0838-0.

[15] M. Ruba, I. A. Viorel, L. Szabó. "Modular stator switched reluctance motor for fault tolerant drive systems," IET Electric Power Applications, vol. 7, no. 3, 2013, pp. 159–169. ISSN 1751-8660.

[16] G. Oriti, A. L. Julian, T. A. Lipo. "An inverter/motor drive with common mode voltage elimination," in IEEE Industry Application Society Annual Meeting, New Orleans, Louisiana, 5–9 October 1997, pp. 587–592.

[17] M. Jones, S. N. Vukosavic, E. Levi, A. Iqbal. "A six-phase series connected two-motor drive with decoupled dynamic control," IEEE Transactions on Industry Applications, vol. 41, no. 4, 2005, pp. 1056–1066.

[18] M. B. R. de Correea, C. B. Jacobina, E. R. C. da Silva, E. M. N. Lima. "An induction motor drive system with improved fault tolerance," IEEE Transactions on Industry Applications, vol. 37, no. 3, 2001, pp. 873–879.

[19] N. Bianchi, S. Bolognani, M. Zigliotto, M. Zordan. "Innovative remedial strategies for inverter faults in IPM synchronous motor drives," IEEE Transactions on Energy Conversion, vol. 18, no. 2, 2003, pp. 306–314.

[20] W. Ouyang, T. A. Lipo. "Modular permanent magnet with fault tolerant capability," in 24th Annual IEEE Applied Power Electronics Conference and Exposition, 2009, pp. 930–937.

[21] C. H. Sneessens, T. Labbe, F. Baudart, F. Labrique, E. Matagne. "Modelling and torque control of a five-phase permanent magnet synchronous motor using tooth concentrated winding technology," in Electromotion 2009, 8th International Symposium on Advanced Electromechanical Motion Systems & Electric Drives Joint Symposium, 2009, pp. 1–6.

[22] M. J. Duran, F. Barrero, S. Toral. "Multi-phase space vector pulse width modulation: applications and strategies," in International Conference on Renewable Energies and Power Quality, 2007, paper ID 341.

[23] A. Akrad, M. Hilairet, D. Diallo. "Design of fault-tolerant controller based on observers for a PMSM drive," IEEE Transactions on Industrial Electronics, vol. 58, no. 4, 2011, pp. 1416–1427.

[24] M. Blanke, M. Kinnaert, J. Lunze, M. Staroswiecki. "Diagnosis and Fault-Tolerant Control." Springer, 2nd ed., 2006, XIX, 672 p. 270 illus.

[25] D. Fodorean, F. Jurca, M. Ruba, D. C. Popa. "Motorization Variants for Light Electric Vehicles—Design, Magnetic, Mechanical and Thermal Aspects." Alma Mater, Cluj Napoca, Romania, 2013. ISBN 978-606-504-160-8